Supporting Information for "Source time function clustering reveals patterns in earthquake dynamics"

Jiuxun Yin[1], Zefeng Li[2], Marine Denolle[1]

[1]Department of Earth and Planetary Sciences, Harvard University, Cambridge, MA, USA

[2]Seismological Laboratory, Division of Geological and Planetary Sciences, California Institute of Technology, Pasadena, CA, USA

Contents of this file

Introduction

In the supporting information for "Source time function clustering reveals patterns in earthquake dynamics", we present additional information on the methods and results. First we provide supplementary information about the clustering of SCARDEC STFs (Text S1, Figures S1 – S6). Second we provide detailed information about the dynamic simulation (Text S2, Figures S7-S12).

Text S1. Dynamic Time Warping clustering of STFs

We downloaded the global catalog of STFs from 3529 $M_W \geq 5.5$ earthquakes from SCARDEC source time function database (`http://scardec.projects.sismo.ipgp.fr`, last accessed 01/20/2020). In this database, there are two types of STFs, average and optimal. In this study, we use the average STFs because their time derivative are not discontinuous. All STFs are resampled over 100 points. The purpose of this step is to retain signals at periods as short at 1 s, while it is not required for the DTW stretching. We also have tested resampling at 200 and 500 points, but our results are insensitive to the number of points. Finally, all STFs are normalized by the seismic moment.

DTW searches for the best point-to-point match between two STFs (Figure S1 (a)) to match their general shapes. The best corresponding relation (white line in Figure S1 (b)) provides an optimal warping/stretching path, along which two STFs can be stretched to the best similarity. The DTW distance is the Euclidian norm once both STFs are warped. Single linkage hierarchical clustering is applied to the DTW distances to build the "family tree" for the entire STF database. 20 clusters are finally determined to keep the rich variations of STF complexity without diving into numerous individual shapes (Figure S1 (c)).

Text S2. Dynamic rupture simulations

Our dynamic simulations are similar with those in (Danré et al., 2019), with slight modification in the pre-stress distribution and in the range of values of frictional parameters. We solve the elastodynamic equations of a mode III fracture with linear slip-weakening friction in a homogeneous infinite medium using the spectral boundary integral methods (SBIEMLAB, code developed by Jean-Paul Ampuero, `http://web.gps.caltech.edu/~ampuero/software.html`, last accessed 11/27/2018).

The total length of simulation domain is fixed as 400 km, but the length of the "fault" where rupture can occur is 200 km. Basic material properties are: P wave velocity V_p = 6.00 km/s; shear wave velocity V_s=3.46 km/s; density ρ=2.67 kg/m^3; shear modulus G=32 GPa and we fix the normal stress σ_0=120 MPa. The linear slip weakening friction is used as a simple but general constitutive relation:

$$\mu = \begin{cases} \frac{(\mu_d - \mu_s)d}{D_c} + \mu_s, d \leq D_c, \\ \mu_d, d > D_c, \end{cases} \tag{1}$$

where d is slip, dynamic friction μ_d=0.525, static friction μ_s=0.677. We vary the characteristic slip weakening distance D_c = 0.05, 0.1, 0.2, 0.4, 0.8, 1.6 m. The nucleation length L_c relates to D_c:

$$L_c = \frac{1.158 G D_c}{(\mu_s - \mu_d)\sigma_0}, \tag{2}$$

which varies from 101.6 to 3250.5 m (Uenishi & Rice, 2003). In our simulations, we set the nucleation patch to be 10 km in extent, which is at least $3L_c$ to guarantee the successful nucleation. The cohesive zone size is:

$$\Lambda_0 = \frac{9\pi}{32} \frac{G}{1-\nu} \frac{D_c}{(\mu_s - \mu_d)\sigma_0}, \tag{3}$$

which varies from 103.3 to 3306.9 m and where $\nu = 0.25$ is the Poisson ratio (Day et al., 2005). To guarantee sufficient spatial resolution, we require spatial sampling along the fault axis x of $\Delta x \leq \Lambda_0/2$ at least for each D_c value.

To generate diverse dynamic ruptures, and their corresponding STFs, we generate statistically similar shear pre-stress $\tau_0(x)$ distributions on the fault plane. To a constant level of shear stress, which equals to the dynamic friction $\mu_d\sigma_0$, we add a perturbation $d\tau_0(x)$, such that the pre-stress is:

$$\tau_0(x) = \mu_d\sigma_0 + d\tau_0(x). \tag{4}$$

The power spectral density (PSD) of $d\tau_0(x)$, $d\mathrm{T}_0(k)$, follows power-law decay in the wavenumber domain,

$$d\mathrm{T}_0(k) = C|k|^{-\gamma}, \tag{5}$$

where $\gamma = 0.8$ is based on observational constraints on the self-afine fault roughness (Dunham et al., 2011; Candela et al., 2012), and C is a normalization factor. Combining the PSD $d\mathrm{T}_0(k)$ with the random phases $\phi(k)$, which are taken from a uniform distribution in $[0, 2\pi]$, we can generate various pre-stress distributions. For each realization of a pre-stress perturbation, we further scale the pre-stress perturbation amplitude to vary within the range from $-0.6(\mu_s - \mu_d)\sigma_0$ to $0.8(\mu_s - \mu_d)\sigma_0$. Finally, we apply a Tukey-window to taper the 100 km on either end of the 400 km pre-stress distributions; this avoids the artifacts in STF from abruptly stopping of rupture at the fault boundary in the spectral boundary integral solutions (Figure S7).

To nucleate spontaneous dynamic ruptures, we apply a weakening nucleation. For each pre-stress distribution, we first perform a peak detection of $\tau_0(x)$ to find its absolute maximum τ_0^{max} within within [-50 50] km. Then, we reduce the fault strength $\tau_s = \tau_0^{max} - 4\mathrm{MPa}$ within a 10 km nucleation region centered at this point, and set $D_c = 0.1$ m in this nucleation region.

For simulations with different D_c values, we keep the identical nucleation processes by fixing the $D_c = 0.1$ m within the nucleation zone. This is to minimize the effects from

nucleation on the STFs. Once nucleated, slip and stresses evolve according to elastodynamics.

We repeat the workflow above to generate diverse ruptures. We remove those that unsuccessfully nucleated (L $\leq$ 20 km) or over-ruptured (those that ruptured over the heterogeneous area at $\pm$ 100 km in Figure S7). We run a sufficient number of ruptures in order to keep 800 qualified dynamic rupture models for each D_c value. We then apply the same approach as in the case of the observations (Figures S8-S12) to cluster those synthetic STFs based on their complexities.

References

Brune, J. N. (1971). Correction (to Brune, 1970). *J. geophys. Res*, *76*, 5002.

Candela, T., Renard, F., Klinger, Y., Mair, K., Schmittbuhl, J., & Brodsky, E. E. (2012). Roughness of fault surfaces over nine decades of length scales. *Journal of Geophysical Research: Solid Earth*, *117*(B8). doi: 10.1029/2011JB009041

Danré, P., Yin, J., Lipovsky, B. P., & Denolle, M. A. (2019). Earthquakes Within Earthquakes: Patterns in Rupture Complexity. *Geophysical Research Letters*, *46*(13), 7352–7360. doi: 10.1029/2019GL083093

Day, S. M., Dalguer, L. A., Lapusta, N., & Liu, Y. (2005). Comparison of finite difference and boundary integral solutions to three-dimensional spontaneous rupture. *Journal of Geophysical Research: Solid Earth*, *110*(B12). doi: 10.1029/2005JB003813

Dunham, E. M., Belanger, D., Cong, L., & Kozdon, J. E. (2011). Earthquake Ruptures with Strongly Rate-Weakening Friction and Off-Fault Plasticity, Part 2: Nonplanar FaultsEarthquake Ruptures with Rate-Weakening Friction and Off-Fault Plasticity, Part 2: Nonplanar Faults. *Bulletin of the Seismological Society of America*, *101*(5), 2308–2322. doi: 10.1785/0120100076

Eshelby, J. D. (1957). The determination of the elastic field of an ellipsoidal inclusion, and related problems. In *Proceedings of the Royal Society of London A: Mathematical, Physical and Engineering Sciences* (Vol. 241, pp. 376–396). The Royal Society.

Noda, H., Lapusta, N., & Kanamori, H. (2013). Comparison of average stress drop measures for ruptures with heterogeneous stress change and implications for earthquake physics. *Geophysical Journal International*, *193*(3), 1691–1712. doi: 10.1093/gji/ggt074

Uenishi, K., & Rice, J. R. (2003). Universal nucleation length for slip-weakening rupture instability under nonuniform fault loading. *Journal of Geophysical Research: Solid*

Earth, *108*(B1), 2042. doi: 10.1029/2001JB001681

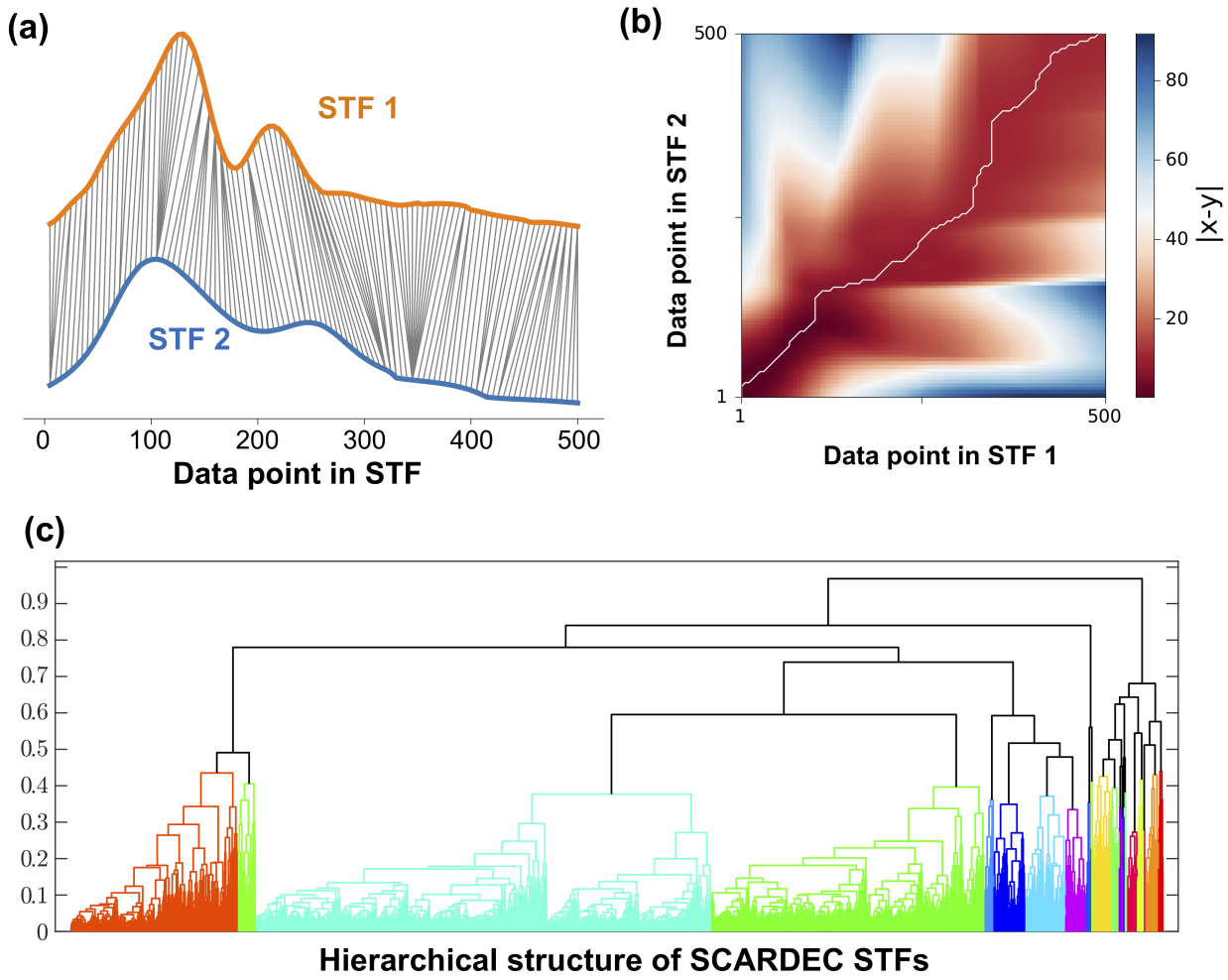

Figure S1. Dynamic time warping (DTW) clustering of earthquake source time functions (STFs). (a) Point-to-point correspondence between two example STFs. (b) Optimal stretching path (white line) from the minimum differences for the two example STFs. (c) Hierarchical structure of all SCARDEC STFs from the DTW clustering.

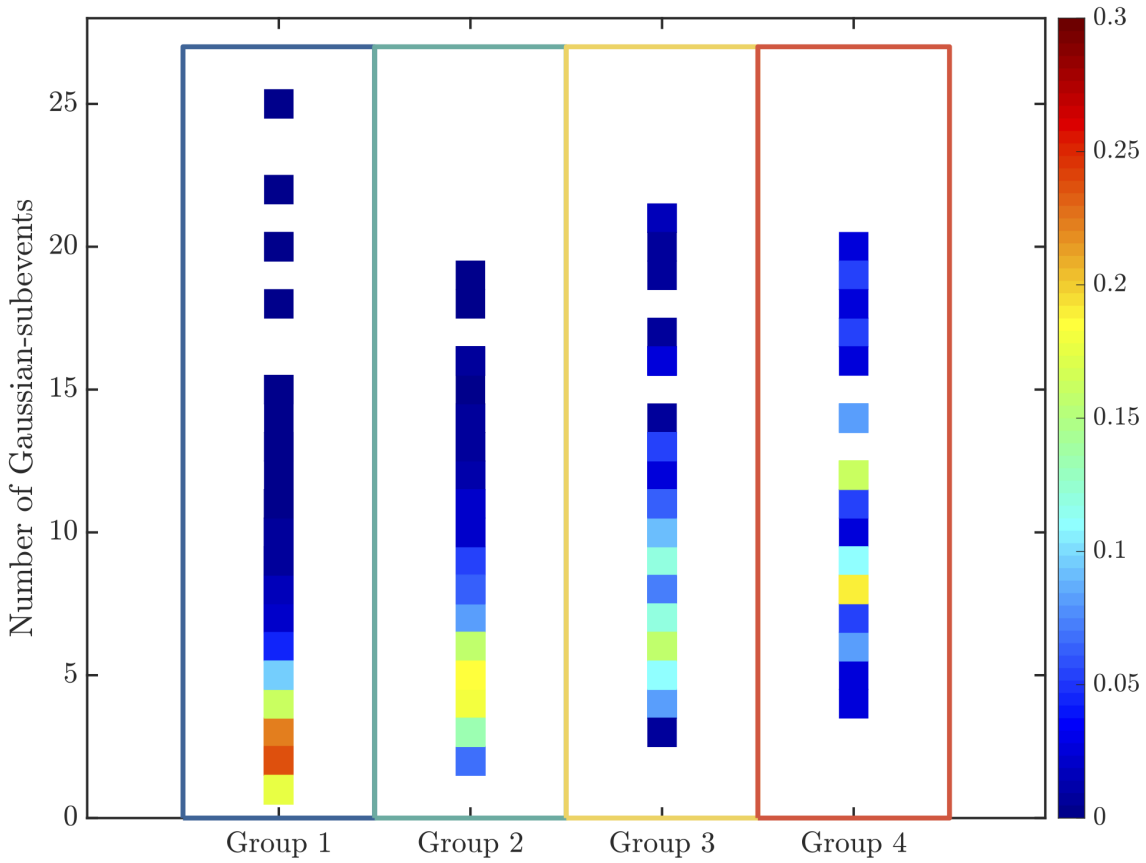

Figure S2. Comparison between the DTW complexity groups and number of Gaussian subevents (Danré et al., 2019). The color indicates the frequency of occurrence within each group.

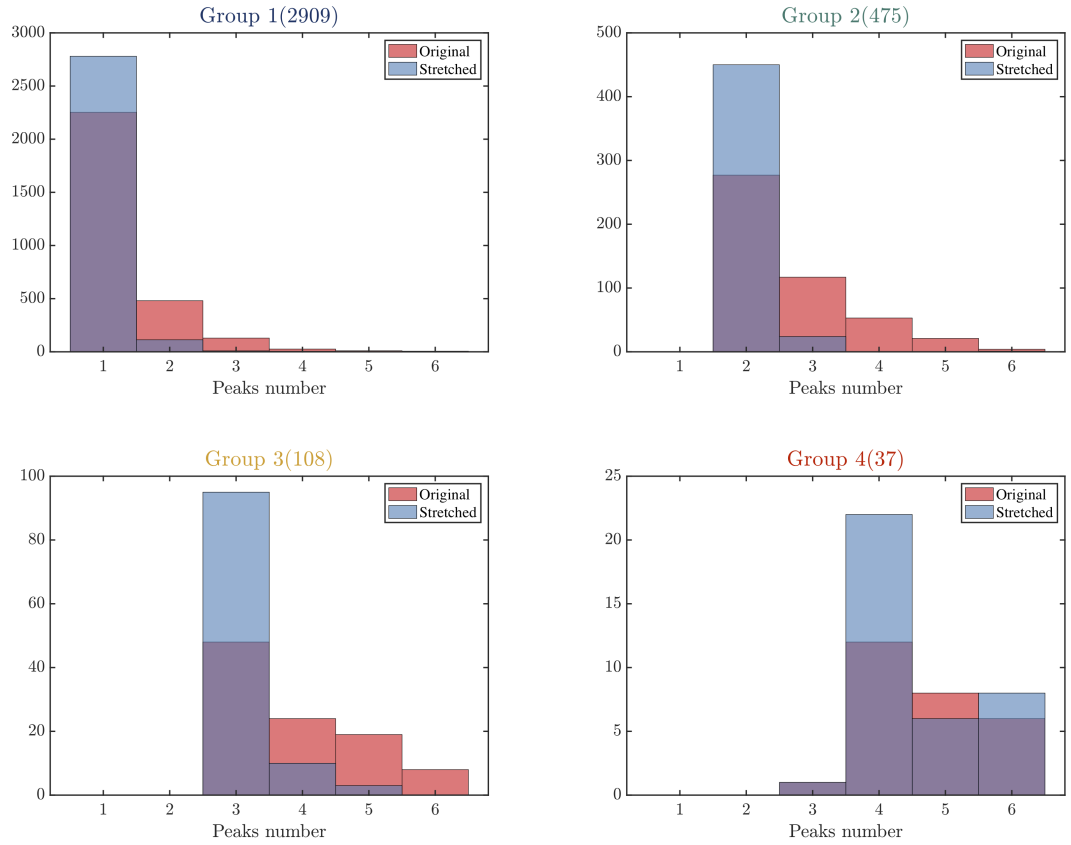

Figure S3. Comparisons between prominent peak (0.1 of STF global maximum) number distributions of original raw STFs (red histograms) and DTW stretched STFs (blue histograms) in each group. Group numbers are also the prominent peak numbers of the centroid event within each group.

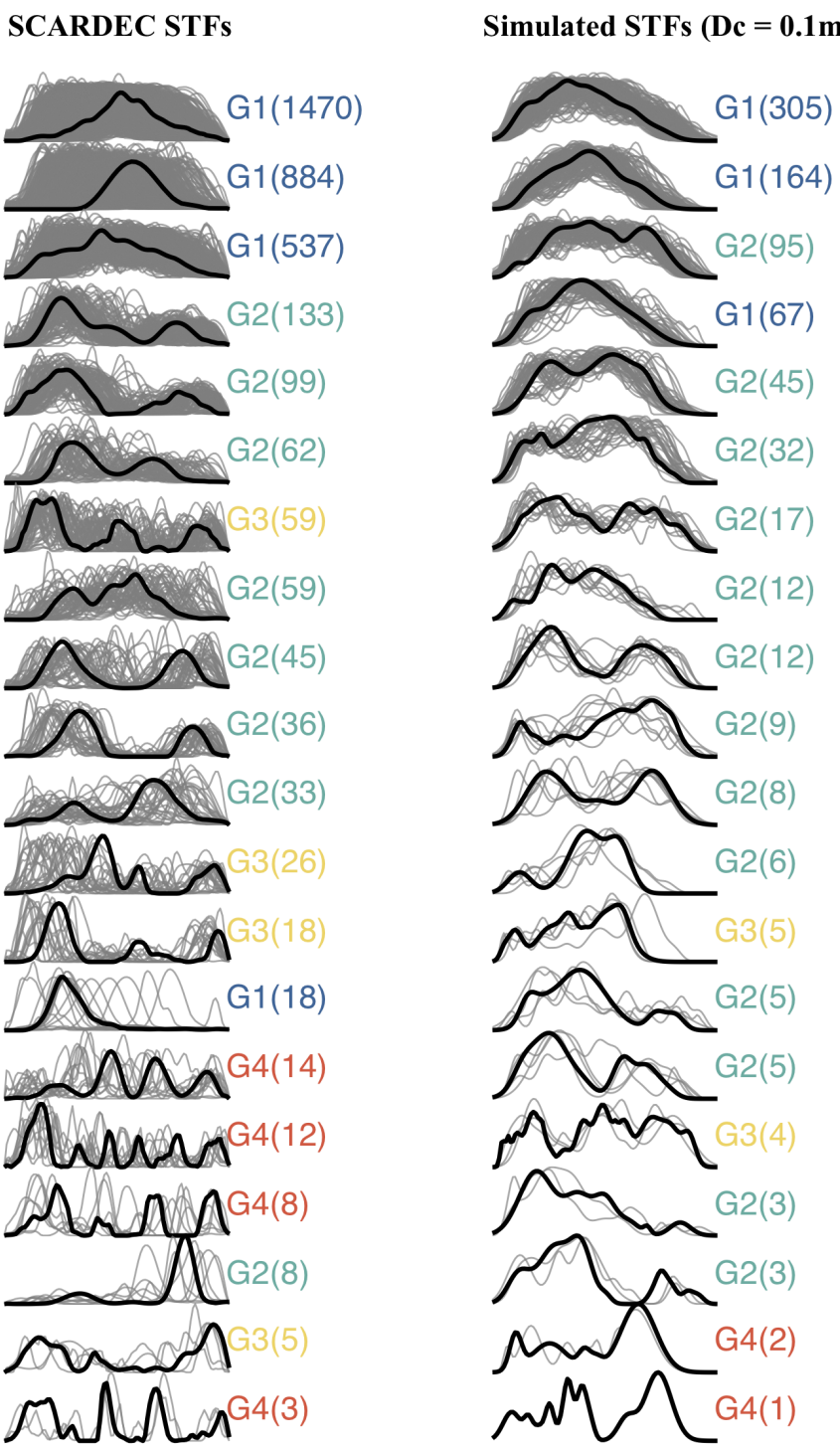

Figure S4. All the STFs before DTW stretching (gray thin lines) compared with the centroid STF (Black thick lines). Other symbols are the same as Figure 1. SCARDEC STFs are shown to the left and simulated STFs ($D_c = 0.1$ m) are shown to the right.

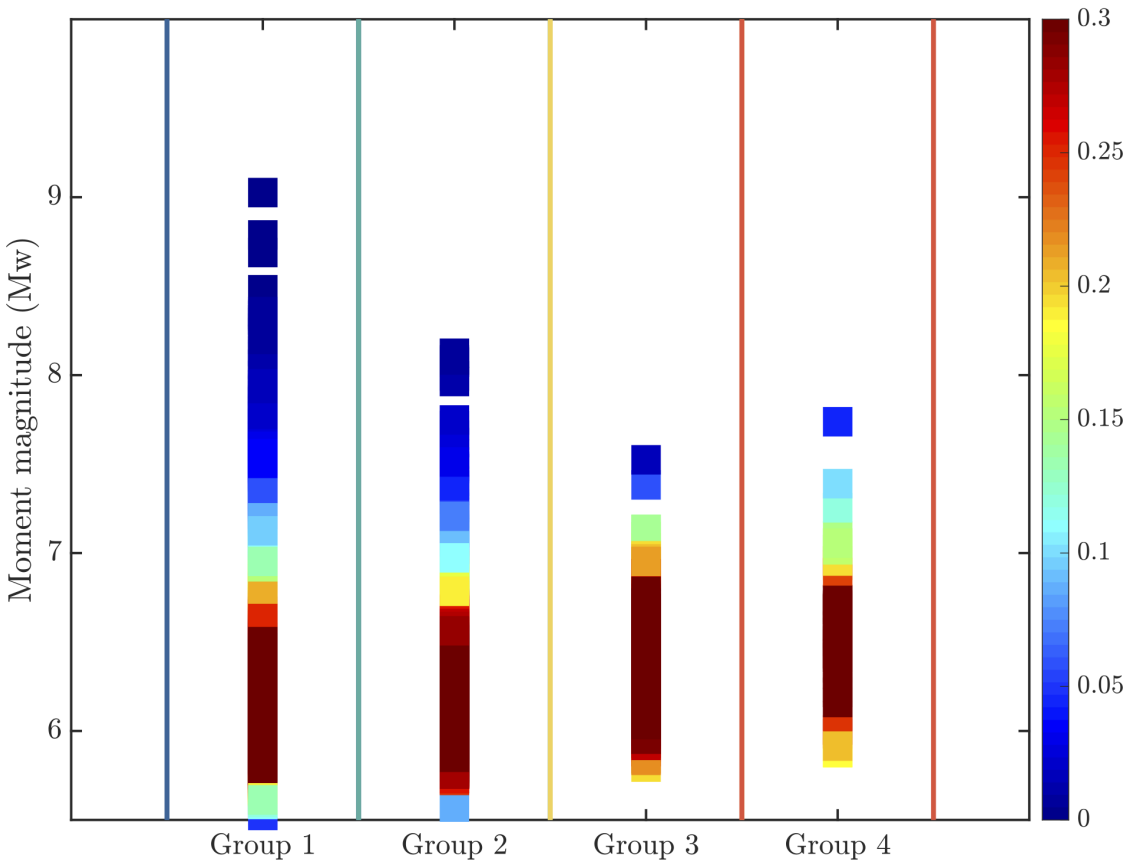

Figure S5. Moment magnitude distributions of the STFs in each group. The color indicates the frequency of occurrence within each group.

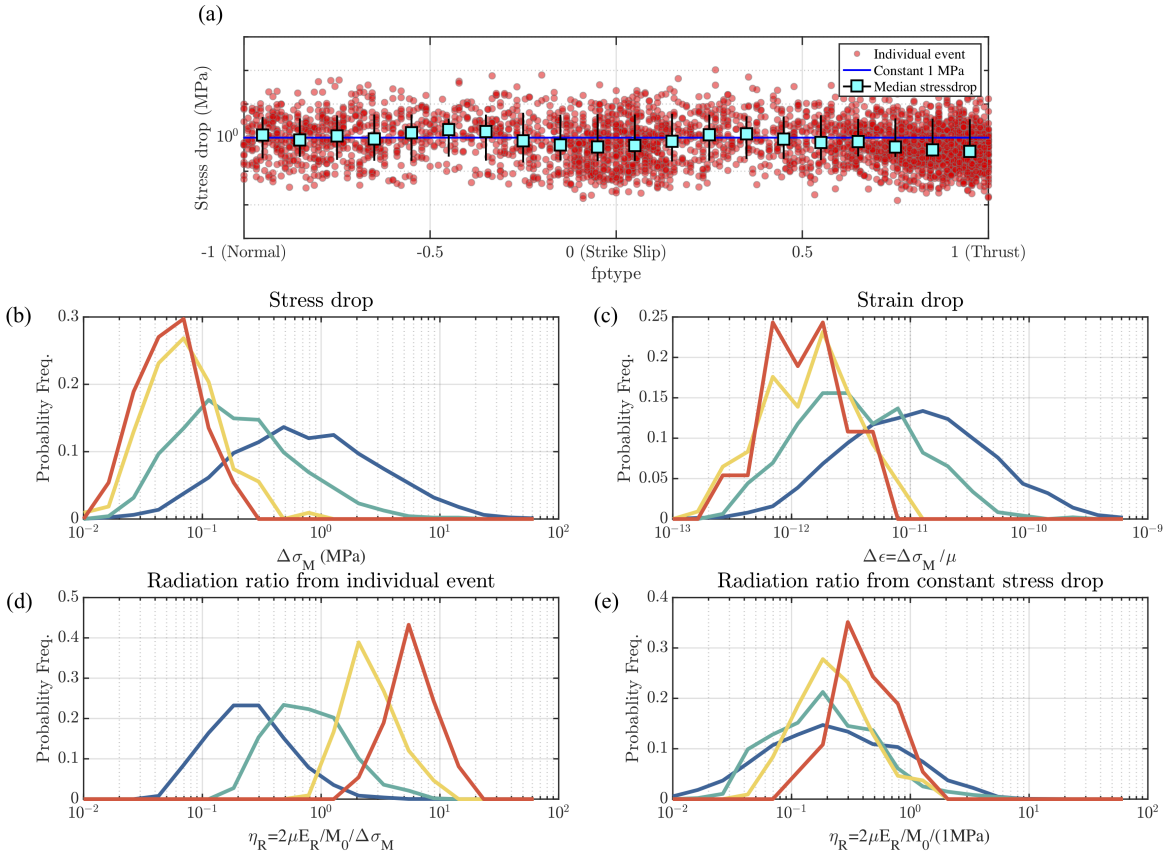

Figure S6. Seismic stress drop estimation using the earthquake duration T_D for each individual earthquake in the SCARDEC database: Panel (a) shows the stress drop variations with focal mechanisms parameters, the stress drop is calculated as $\Delta\tau = 7/16M_0/(0.32V_sT_D)^3$ (Eshelby, 1957; Brune, 1971). In the dynamic simulation, the average stress drop of all models is approximately 1 MPa. Panel (b) shows the group distributions of estimated stress drop based on event duration. (c) and (d) show the group distributions of corresponding strain drop and radiation ratio calculated from stress drop, respectively. Note that the stress drop estimation based on duration is model-dependent and may be underestimated for the very heterogeneous earthquake rupture (Noda et al., 2013), such as the complex Group 3 and Group 4, thus leads to very high radiation efficiency. Panel (e) also shows the group distributions of radiation ratio, but estimated based on the assumption that stress drop is a constant value of 1 MPa, for comparison.

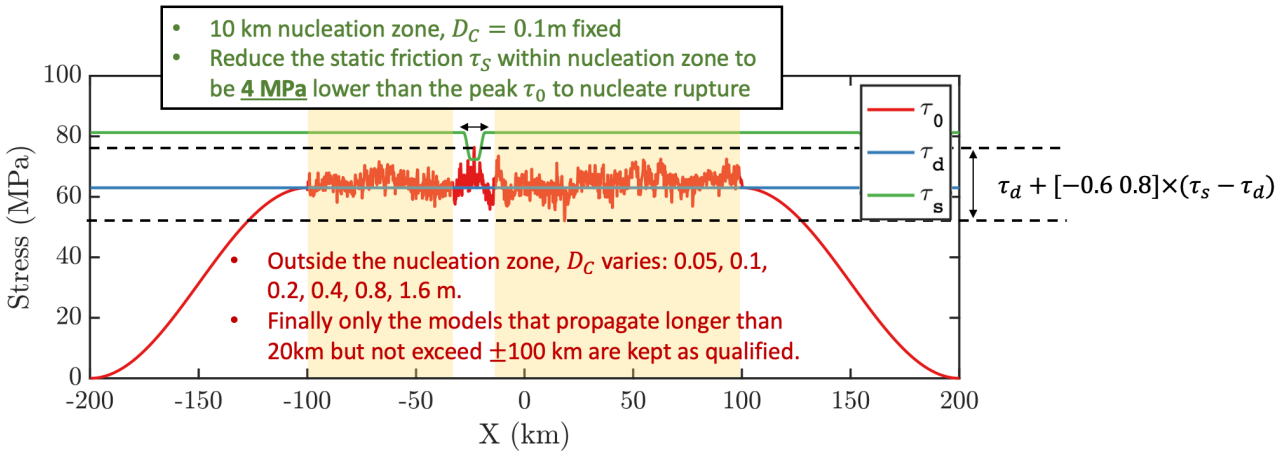

Figure S7. Pre-stress (red curve) and frictional strengths (green curve: static friction; blue curve: dynamic friction) settings of the dynamic rupture simulations. Dashed lines indicate range of values of the randomly generated pre-stress. Finally, only the rupture models terminates within the yellow shadow regions are kept as the qualified models.

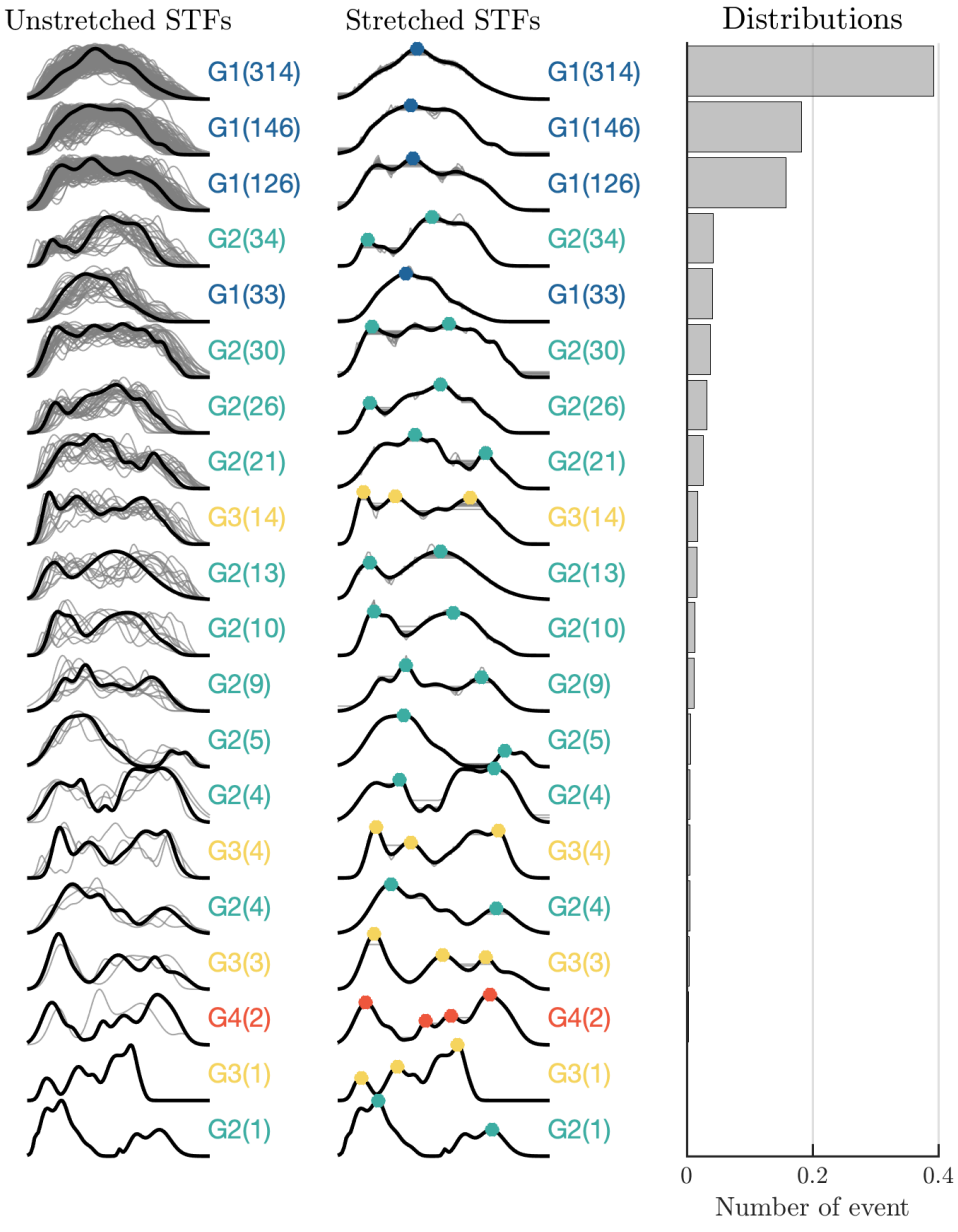

Figure S8. DTW clustering results for the simulated STFs with $D_c = 0.05$ m.

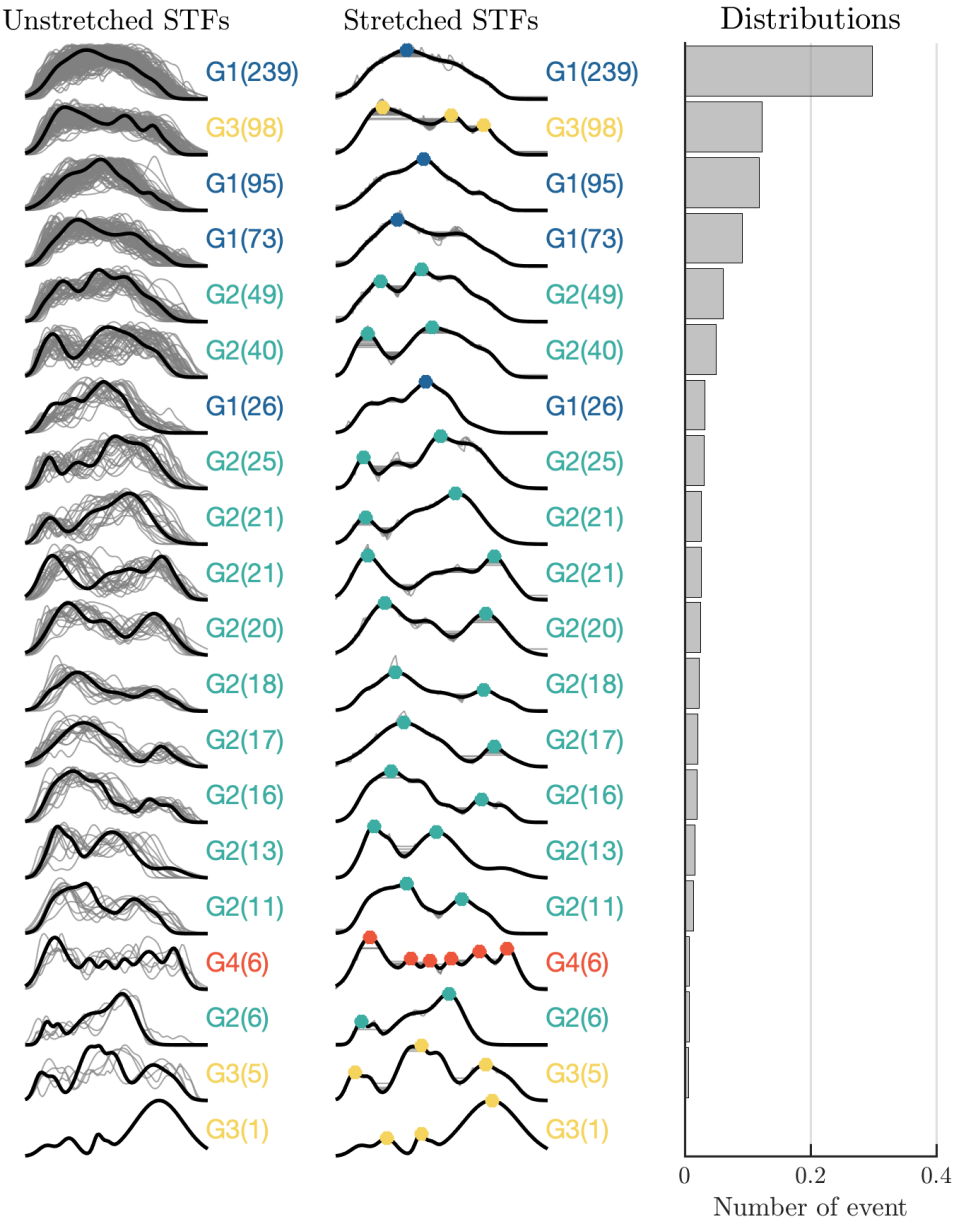

Figure S9. DTW clustering results for the simulated STFs with $D_c = 0.2$ m.

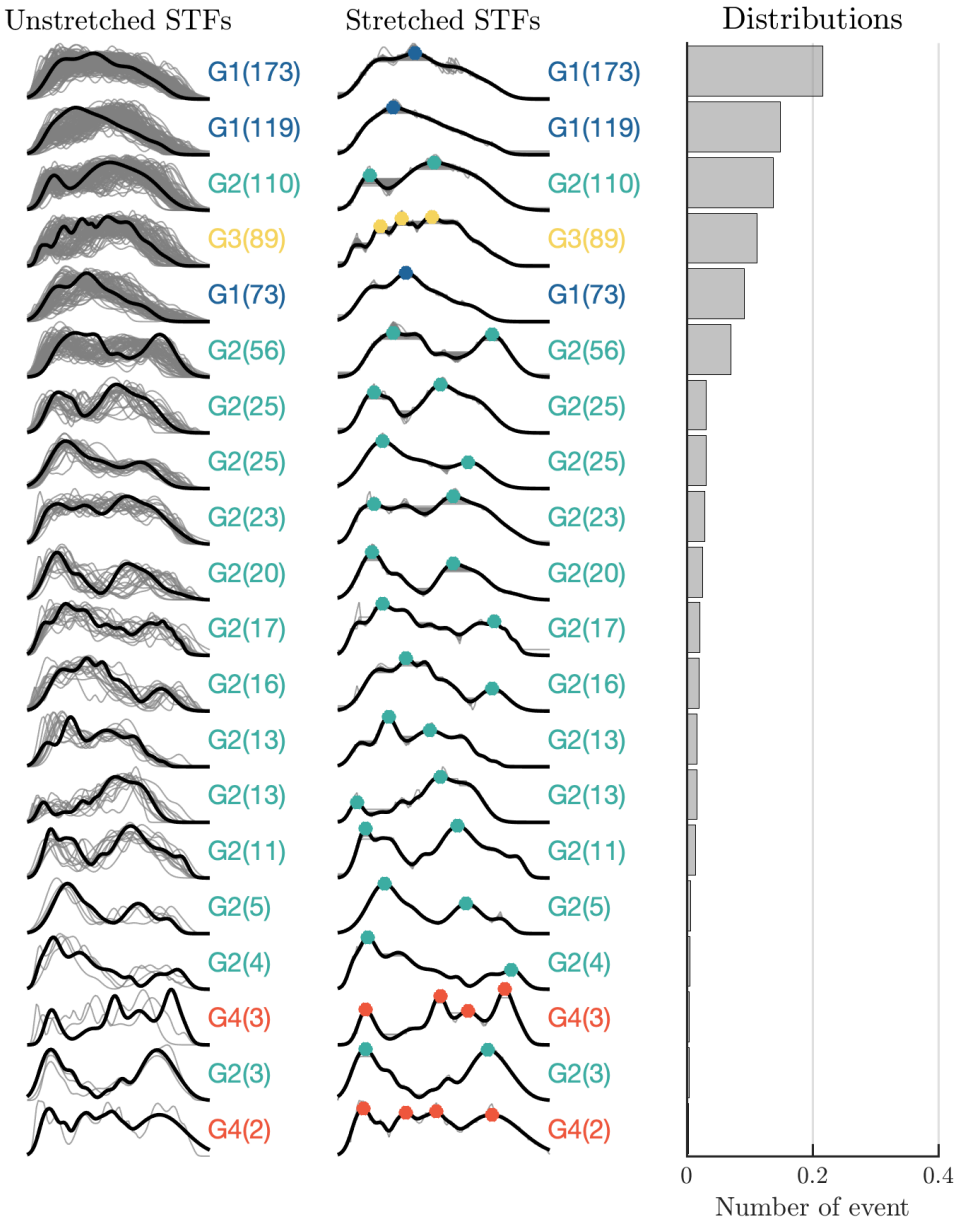

Figure S10. DTW clustering results for the simulated STFs with $D_c = 0.4$ m.

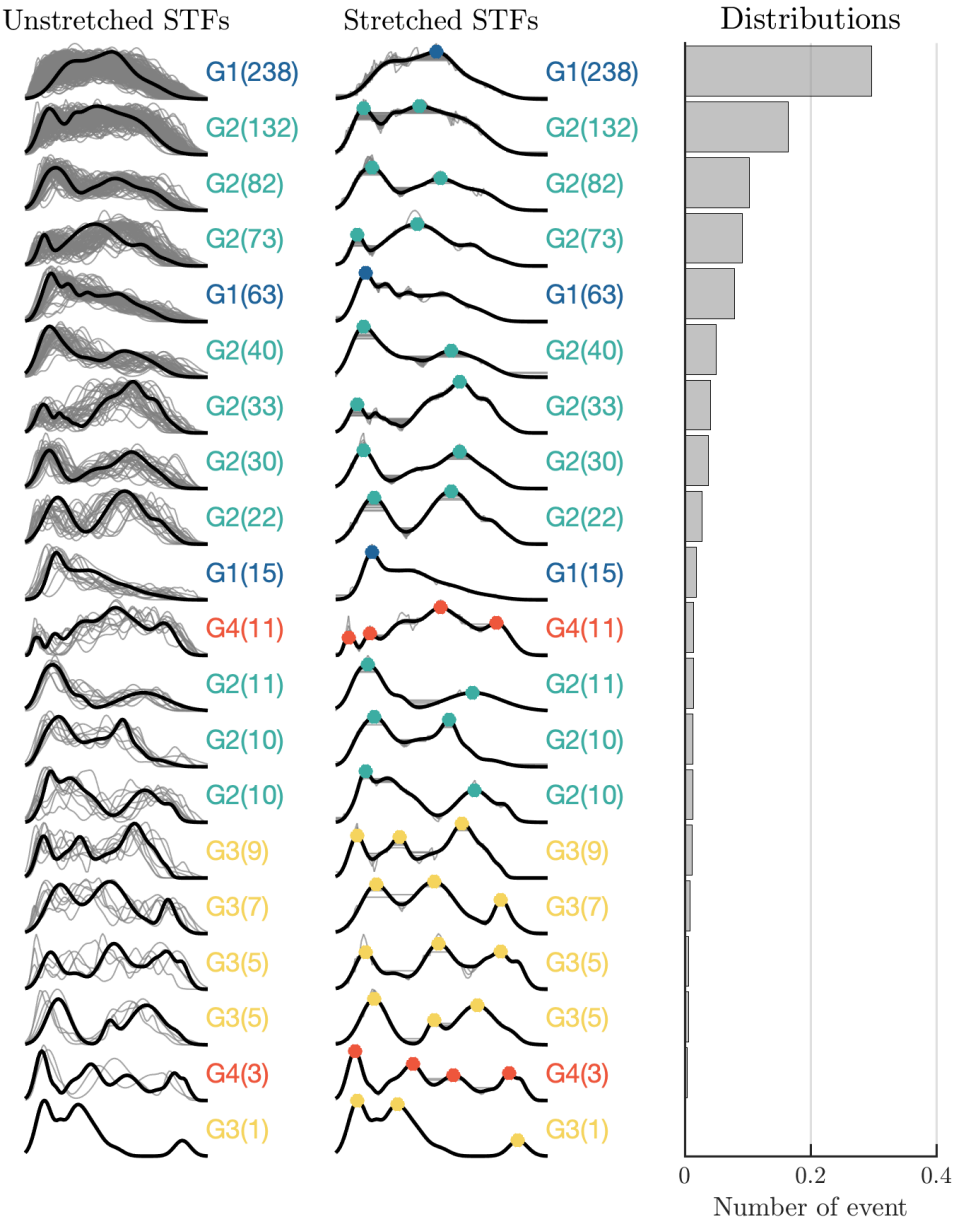

Figure S11. DTW clustering results for the simulated STFs with $D_c = 0.8$ m.

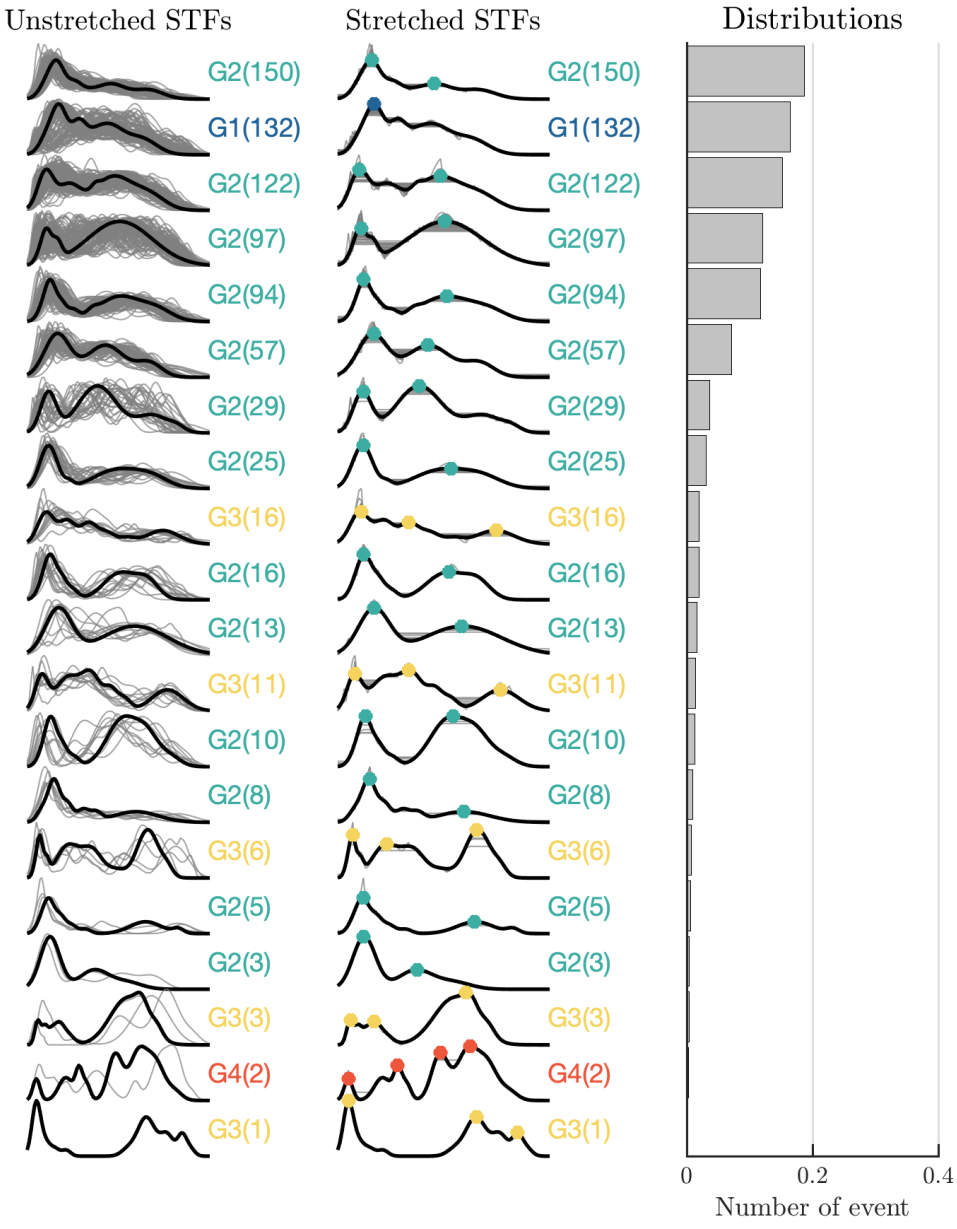

Figure S12. DTW clustering results for the simulated STFs with $D_c = 1.6$ m.